Article

JOURNAL OF THE CHINESE CHEMICAL SOCIETY

A Green Route to Produce Adipic Acid on TiO_2–Fe_2O_3 Nanocomposites

Nawal Ameur,* Redouane Bachir, Sumeya Bedrane and Abderrahim Choukchou-Braham

Laboratory of Catalysis and Synthesis in Organic Chemistry (LCSCO), University of Tlemcen, Tlemcen, Algeria

(Received: April 10, 2017; Accepted: June 16, 2017; DOI: 10.1002/jccs.201700130)

In this work, we study cyclohexene oxidation by molecular oxygen on doped-TiO_2. The improvement of the oxidizing capacity of titanium oxide by doping with iron oxide at different molar ratios is checked. All materials with different molar ratios (Ti/Fe = 9, 4, and 2) are prepared by the sol–gel method and fully characterized by ICP, XRD, SEM, DR/UV–vis, IR, and N_2 adsorption/desorption. The results show that iron is successfully incorporated into the titanium matrix but the incorporated amount is limited. In catalytic tests, improved activity is noticed while using TiO_2 in the presence of Fe_2O_3, which is due the improved oxidation. Conversion in the range of 21–42% depending on the presence of iron oxide was obtained with excellent yield of adipic acid (97% selectivity).

Keywords: Cyclohexene oxidation; Nanocomposite; Adipic acid; Iron; Titania.

INTRODUCTION

The oxidation of alkenes to value-added chemicals has recently received much attention.[1–4] The resulting products from this reaction attract a lot of interest because of their use in the manufacture of perfumes, pharmaceuticals, dyestuff, and agrochemicals.[5–10]

Different products can be obtained from cyclohexene oxidation, but it is difficult to control the product selectivity in this case. This is due to the existence of two active bonds in this molecule. (1) The oxidation of the C–H bond takes place at the allylic position, which is responsible for the formation of cyclohexene hydroperoxide, 2-cyclohexene-1-ol, and 2-cyclohexene-1-one, whereas (2) the oxidation of the C=C bond leads to cyclohexene oxide, cyclohexanol, cyclohexanone, and cyclohexane dioladipic acid (Scheme 1).[11–14]

For cyclohexene oxidation, the traditional oxidants are *t*-butyl hydroperoxide, H_2O_2, and molecular oxygen, the last one being the greenest and the most abundant.[3,14–18] Cyclohexene oxidation with H_2O_2 is another alternative to producing adipic acid (Scheme 2), which is one of the most widely used dicarboxylic acids in the chemical industry. It can be also used for the manufacture of nylon 6,6 polyamide, polyurethanes, plasticizers, and other pharmaceutical chemicals.[12,19–21]

TiO_2 is largely employed to support metal nanoparticles and applied in several photocatalytic reactions and to oxidize hydrocarbons.[22–24] As nanomaterials, TiO_2 (nanoparticles, nanofibers, and nanotubes) demonstrates an interesting behavior in cyclic olefin (1,5-cyclooctadiene, indane, and cyclohexane) oxidation. However, TiO_2 shows conversion in the range of 58–66% depending on titania form, with a noticeable production of unsaturated ketone (62–40%).[25]

TiZrCo catalysts have been studied for the oxidation of cyclohexene by molecular oxygen (2 MPa, 120°C for 12 h). For Ti60Zr10Co30, 92.2% cyclohexene conversion is obtained at 57.6% selectivity for 2-cyclohexen-1-one. The rest may consist of reaction intermediates such as cyclohexene hydrogen peroxide and highly oxidized products such as some ring-opening acids. This result is explained as due to the presence of active species such as CoO and Co_3O_4 on the surface.[26]

In this work, we study the improvement of the oxidation capacity of TiO_2 upon iron addition and the application of these materials in the cyclohexene oxidation reaction by O_2. On one hand, different molar ratios are selected to prepare TiO_2–Fe_2O_3 nanocomposites by the sol–gel method in order to introduce the maximum of quantity iron particles into the titanium matrix. On

*Corresponding author. Email: ameurnawel@yahoo.fr

 © 2017 The Chemical Society Located in Taipei & Wiley-VCH Verlag GmbH & Co. KGaA, Weinheim

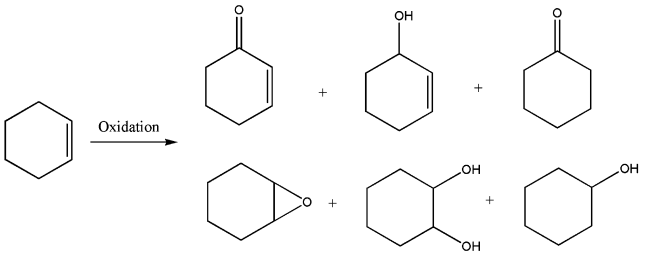

Scheme 1. Cyclohexene oxidation products.

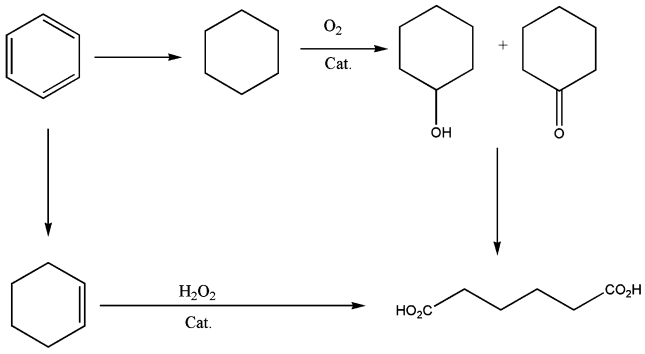

Scheme 2. Two routes for the synthesis of adipic acid.

the other hand, the catalytic performance of the prepared materials is studied in the cyclohexene oxidation by molecular oxygen.

RESULTS AND DISCUSSION

The chemical composition and the surface properties of the prepared materials are summarized in Table 1. We observe that the amount of iron incorporated into the materials depends on the initial Ti/Fe ratio. Thus, we notice that, with the increase of the initial quantity of iron, the incorporated amount in TiO_2 decreases, which may indicate that the maximum incorporation limit is reached.

The N_2 adsorption–desorption isotherms and pore size distribution are shown in Figure 1, and the corresponding physical parameters are summarized in Table 1. All the samples exhibit type IV isotherms typical of mesoporous structures with a sharp inflection at a relative pressure of ~0.5–0.8, a narrow pore size distribution of ~ 7–5 nm, and a H2-type hysteresis.

The X-ray diffraction (XRD) patterns of TiO_2 and TiO_2–Fe_2O_3 materials are shown in Figure 2. These XRD patterns show for titania (a) the presence of peaks at $2\theta = 25.72°$, 38.37°, 48.79°, 54.7°, 55.76°, 63.48°, 69.68°, and 71.23°. These peaks are attributed to the faces (101), (004), (200), (105), (211), (204), (116), and (220), respectively. These peaks confirm that the titania is present only as the anatase phase (tetragonal, $a = b = 3.775$ Å, $c = 9.4912$ Å). In the doped materials, the presence of the anatase diffraction peaks is observed, but a small shift of the maximum of these peaks is noticed in the presence of iron oxide.

For instance, the peak at 25.41° in pure titania is shifted to 25.47°, 25.52°, and 25.49° for TiFe-9, TiFe-4, and TiFe-2, respectively. This phenomenon is observed for all titania peaks and for all materials. This can be related to the formation of a solid solution of iron and titanium oxide. Moreover, the crystallites' average size also decreases with increasing amount of iron, which confirms our previous conclusion.[27]

For TiFe-9 and TiFe-4, we observe a new peak at 30.96° related to the brookite phase. The intensity of this peak increases with the iron amount, indicating that iron oxide catalyzes the transformation of anatase into brookite. Finally, iron particles are also present as the hematite phase (α-Fe_2O_3) at $2\theta = 69.36°$ in TiFe-9, $2\theta = 75.4°$ for TiFe-4, and $2\theta = 69.5°$, and 75.21° for TiFe-2.

The literature indicates that doping titania with lower amounts of Fe_2O_3 is associated with the formation of the anatase phase without any remarkable influence on the crystallite size[28] and that a low amount of Fe_2O_3 is incorporated into the TiO_2 lattice which is attributed to the similarities of the ionic radii of Ti^{4+} and Fe^{3+}.[29]

Table 1. Chemical composition and textural properties of the prepared solids

Material	Moles of Fe/g of oxide × 10^5	Rate of Fe_2O_3 incorporation (%)	Crystallite size (nm)[a]	Pore volume (cm^3/g)	S_{BET} (m^2/g)	Pore diameter (nm)
TiO_2	—	—	12.5	0.28	148	7
TiFe-9	33.2	93	7.0	0.10	87	5
TiFe-4	28.3	40	5.5	0.08	39	5
TiFe-2	38.7	38	5.4	0.08	52	6

[a] Estimated from XRD.

 © 2017 The Chemical Society Located in Taipei & Wiley-VCH Verlag GmbH & Co. KGaA, Weinheim

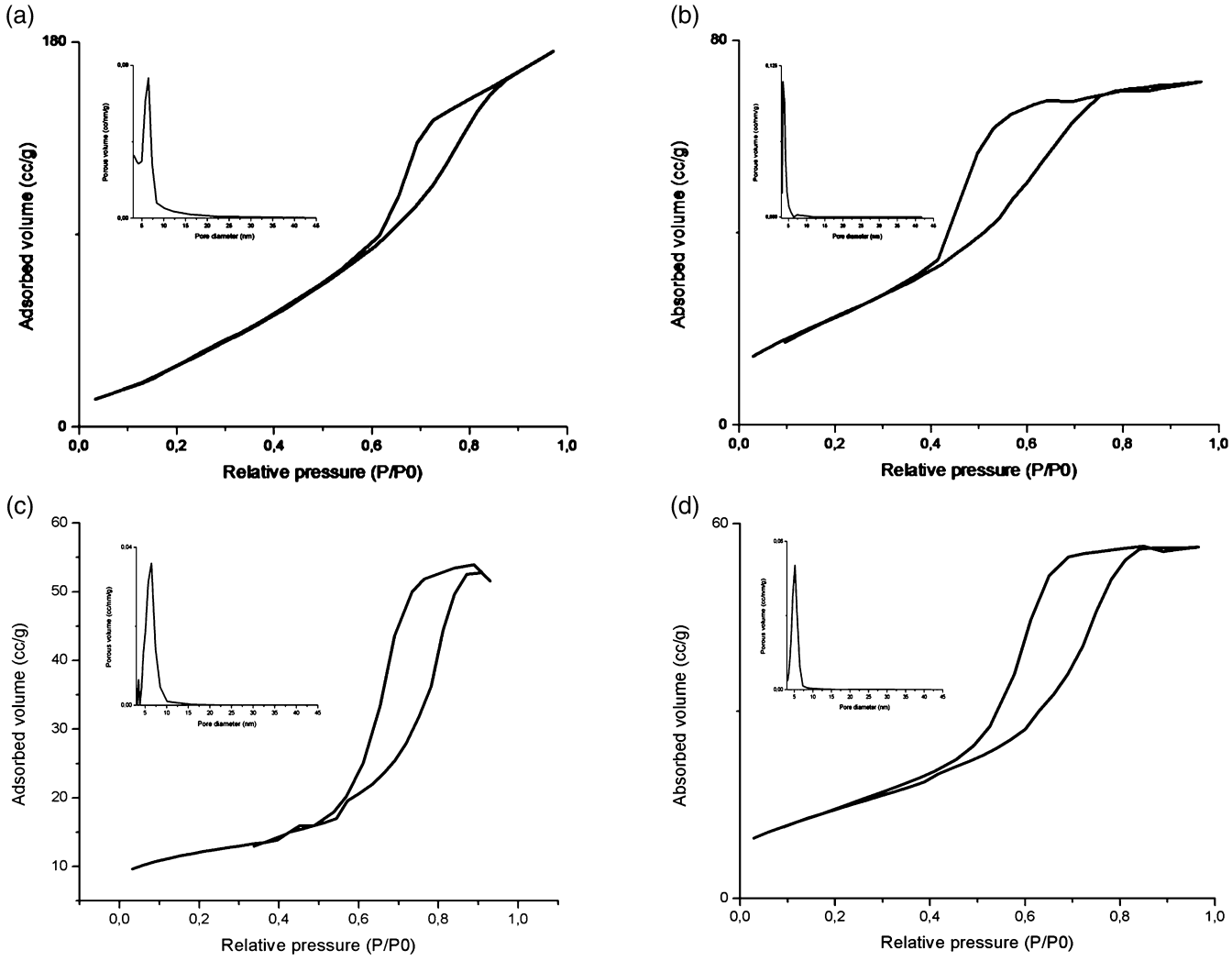

Fig. 1. N_2 adsorption–desorption isotherm of (a) TiO_2, (b) TiFe-9, (c) TiFe-4, and (d) TiFe-2.

However, increasing the amount of iron in titania accelerates the anatase–rutile transformation. This phenomenon is related to the increasing number of Fe^{3+} ions occupying the substitutional positions in the titanium crystal structure.[27]

We can conclude that iron particles were successfully incorporated in the titania matrix and that the excess iron is present as hematite.

TiO_2–Fe_2O_3 materials were also characterized by scanning electron microscopy (SEM). Representative micrographs are shown in Figure 3.

The micrographs confirm good crystallization of the materials under study. We can conclude that the presence of iron in these materials does not seem to change the shape of the particles (Figure 3).

The deconvoluted diffuse reflection (DR)/UV–vis spectra of all prepared samples are shown in Figure 4. The spectrum of TiO_2 showed absorption bands in the range 200–330 nm. The original spectrum was fitted, which revealed three bands at 209, 272, and 326 nm. The first band is due to the ligand–metal charge transfer between Ti^{4+} and ligand (O–H, O–Ti, or H_2O). The second band is related to the Ti^{4+}cations in octahedral environment,[30,31] while the third band due to the anatase phase appears at 326 nm.[31,32]

 © 2017 The Chemical Society Located in Taipei & Wiley-VCH Verlag GmbH & Co. KGaA, Weinheim

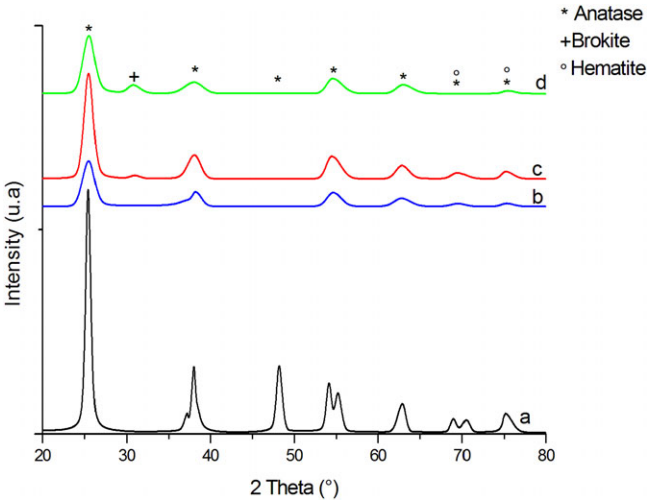

Fig. 2. XRD diffractograms of (a) TiO_2, (b) TiFe-9, (c) TiFe-4, and (d) TiFe-2.

For doped materials, it is noticeable that the spectral intensity increases in the visible region with increase of the Fe content (Figure 4).

Thus, the fitted spectra show three absorption zones:

1. Between 200 and 250 nm: these bands may be related to the anatase phase of titania with comparable intensities and peak positions for all materials. Hence, in the same region, isolated Fe^{3+} cations (charge transfer πd–πp between Fe and O) can appear[33,34]
2. Between 250 and 400 nm: which is assigned to the small $(FeO)n$[33–35]
3. Between 400 and 650 nm: related to larger iron oxide nanoparticles or the polymeric species. A red shift of these bands with the increase of iron content indicates a quantum size effect in these species (Figure 5).[36]

Figure 6 shows the Fourier transform infrared (FTIR) spectra of all materials. The IR spectrum of TiO_2 nanoparticles reveals the presence of major bands centered at 600 cm^{-1}, which are attributed to the stretching vibrations of the Ti–O–Ti group of the anatase phase.[27,37] It can be observed that there are broad peaks at 3300 and 1210–1740 cm^{-1}, assigned to water stretches and bends, respectively.[38,39] For the doped materials, a new band at 1070 cm^{-1} is observed, which corresponds to the vibration of Ti–O–Fe.[27]

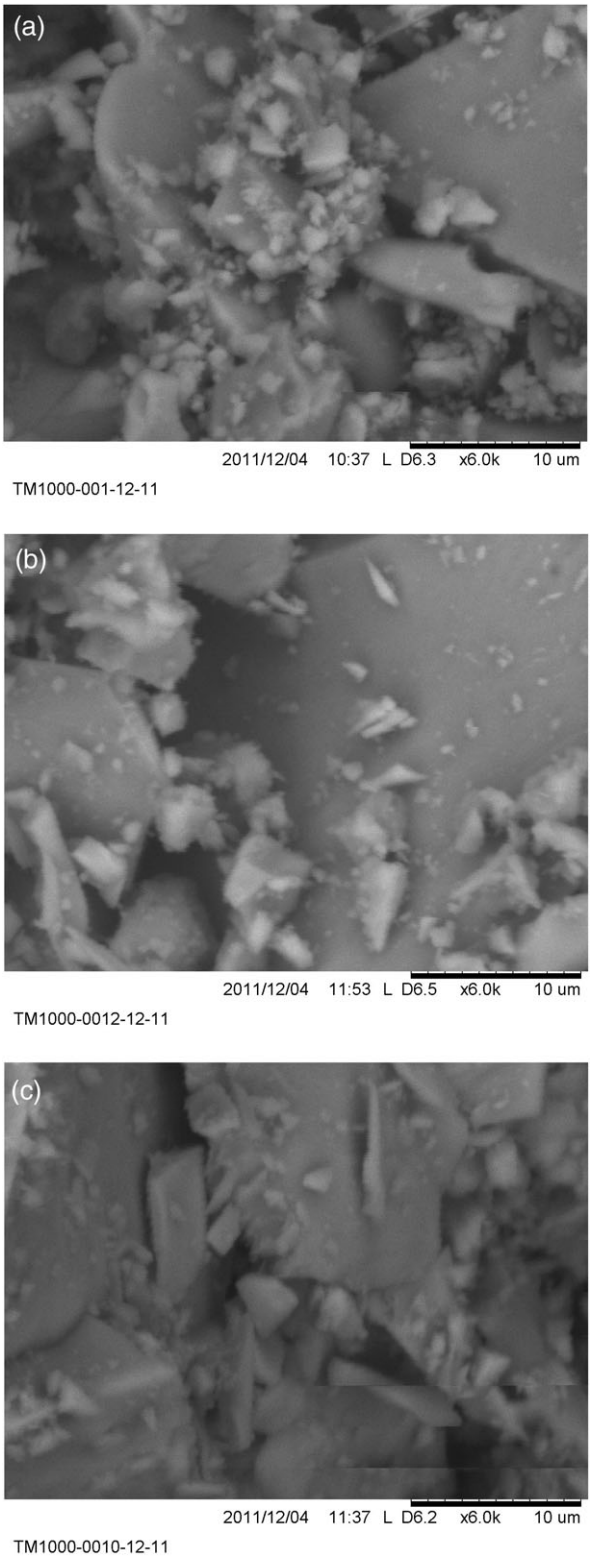

Fig. 3. SEM micrographs of (a) TiFe-9, (b) TiFe-4, and (c) TiFe-2.

 © 2017 The Chemical Society Located in Taipei & Wiley-VCH Verlag GmbH & Co. KGaA, Weinheim

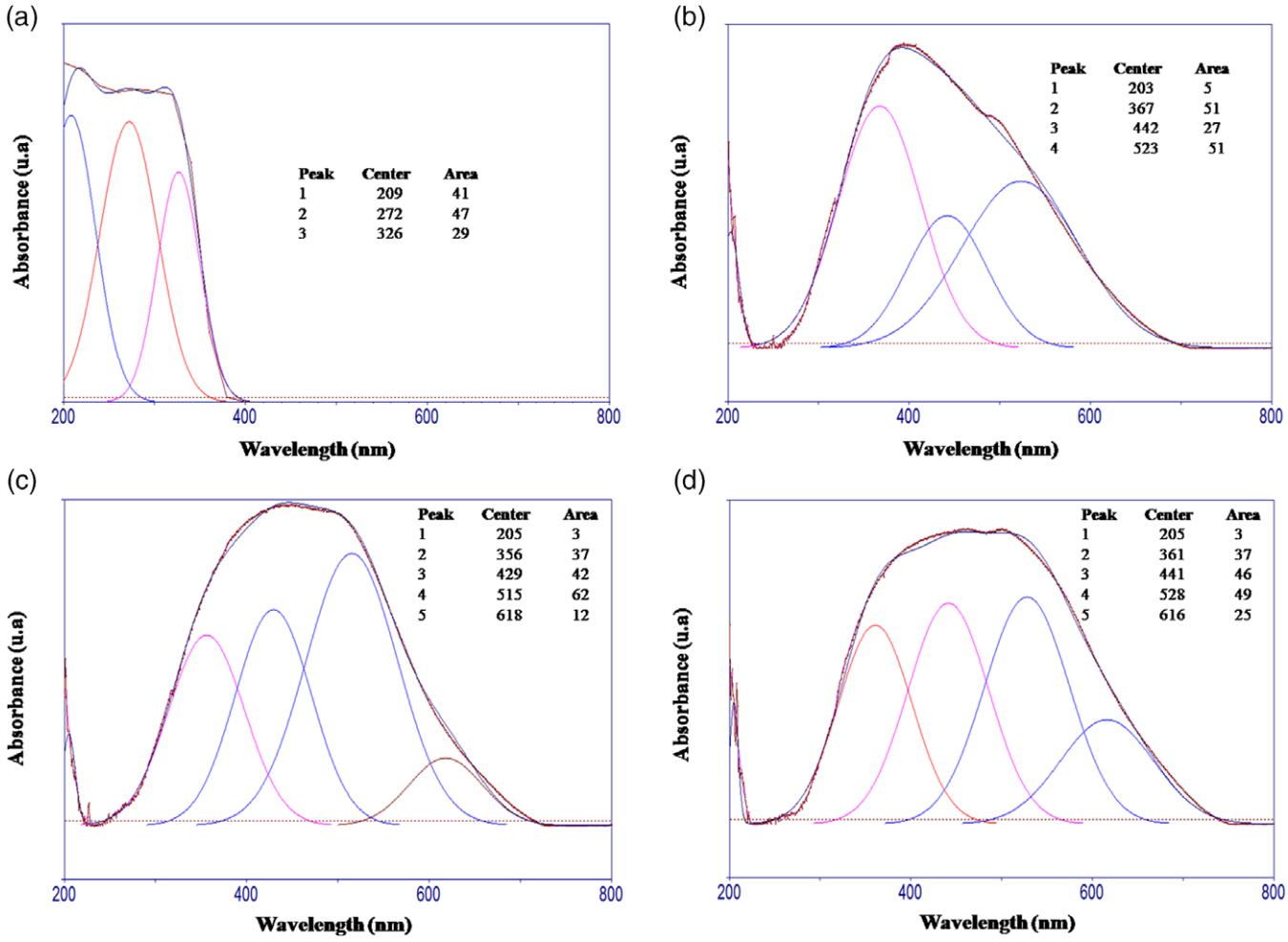

Fig. 4. DR/UV–vis spectral (deconvoluted) bands (a) TiO_2, (b) TiFe-9, (c) TiFe-4, and (d) TiFe-2.

Catalytic performance in the oxidation reaction

The catalytic performance of the TiO_2–Fe_2O_3 catalysts, in comparison with pure TiO_2, is reported in Table 2. Pure titania shows a cyclohexene conversion of 29%. This activity is improved by up to 42% by the addition of iron oxide.

The catalytic performance of titanium oxide appears to be modified on the incorporation of iron particles, which is associated with the changes in the particle structure, size, and consequent oxidant behavior, as described by Prieto-Centurion *et al.*[36]

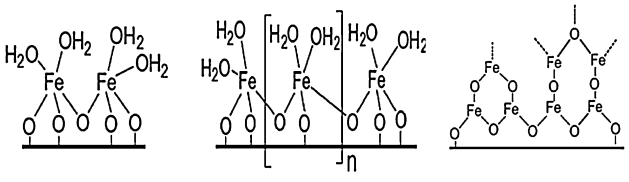

Fig. 5. Iron species on titania surface.

In terms of selectivity, substantial production of adipic acid is obtained for all catalysts (97–95%) independent of the amount of iron oxide (Table 2). It may be concluded that titanium oxide is very selective toward adipic acid and that the presence of iron particles (TiFe-2) improves the overall conversion.

According to the literature,[11,40] cyclohexene oxidation with molecular oxygen, and in the presence of the catalyst, initially forms 2-cyclohexene-1-hydroperoxide. This product is not stable and can decompose into 2-cyclohexene-1-ol and 2-cyclohexene-1-one (step 3), or 2-cyclohexene-1-one and water (step 2) or form cyclohexane oxide and 2-cyclohexene-1-ol (step 4) in presence of a second cyclohexene molecule. Adipic acid

© 2017 The Chemical Society Located in Taipei & Wiley-VCH Verlag GmbH & Co. KGaA, Weinheim

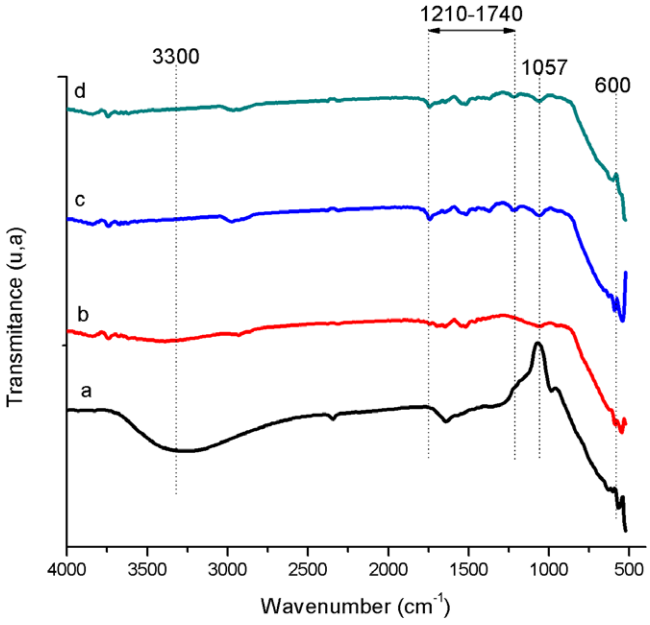

Fig. 6. Infrared spectra of (a) TiO_2, (b) TiFe-9, (c) TiFe-4, and (d) TiFe-2 materials.

is formed by a series of reactions (oxidation and hydrolysis), as shown in Scheme 3.[6]

Although the mechanism is not established, we propose that adipic acid is formed by a one-pot transformation via a five-step scheme involving the hydrolysis of cyclohexane epoxide into cyclohexane-1,2-diol, alcohol oxidation into 2-hydroxycyclohexanone, Baeyer–Villiger oxidation into 7-hydroxyoxepan-2-one, alcohol oxidation into oxepane-2,7-dione, and finally hydrolysis to form adipic acid.[5,13,41]

The literature indicates that appropriate conditions (medium or catalytic acid sites) facilitates the formation of adipic acid and cyclohexene oxidation[14] and that the iron species present as Fe^{3+} improves the

Table 2. Comparison of the catalytic performance of TiO_2 and TiO_2–Fe_2O_3 on cyclohexene oxidation

Catalysts	C (%)[a]	TON (mol/g)	S_{ENONE} (%)[b]	S_{ENOL} (%)[c]	S_A (%)[d]
TiO_2	29	0.2175	02	01	97
TiFe-9	28	0.2100	02	01	97
TiFe-4	21	0.1597	06	02	92
TiFe-2	42	0.3150	02	01	97

[a] Cyclohexene conversion.
[b] Cyclohexen-1,2-enone selectivity.
[c] Cyclohexen-1,2-enol selectivity.
[d] Adipic acid selectivity.

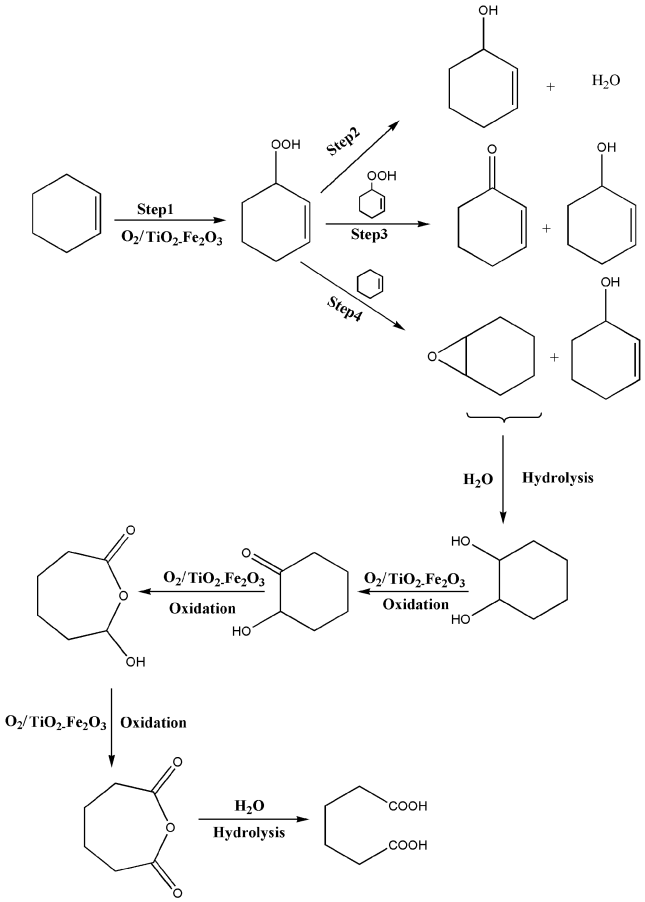

Scheme 3. Proposed mechanism for the formation of the different reaction products from cyclohexene oxidation.

catalytic activity as they are able to activate the C–H bond, which may also promote the O–O hemolytic cleavage.[36]

In this case, we notice that the use of molecular oxygen as oxidant is beneficial for this reaction, as oxygen is a diradical facilitating a number of radical reactions that can be useful for a range of low-temperature oxidations.

CONCLUSIONS

The oxidation process of cyclohexene with molecular oxygen to produce adipic acid was studied on pure and Fe-doped TiO_2. First, the sol–gel method led to binary oxides, where iron species were incorporated into the titania matrix with an average size of 5–11 nm. Excess iron was observed as the hematite phase.

Furthermore, the catalytic activity of the catalysts showed excellent selectivity toward adipic acid

 © 2017 The Chemical Society Located in Taipei & Wiley-VCH Verlag GmbH & Co. KGaA, Weinheim

formation (up to 97%) and improved cyclohexene conversion in the presence of iron oxide in titania. This may be related to the improvement of the oxidation behavior of titania in the presence of the iron species.

EXPERIMENTAL

Material preparation

Different materials (TiO_2–Fe_2O_3) were prepared by the sol–gel method, as described by Kundu *et al.*[42] We selected the following molar ration Ti/Fe = 9, 4, and 2, and the corresponding materials were denoted TiFe-9, TiFe-4, and TiFe-2, respectively. Typically, a corresponding volume of titania precursor (titanium isopropoxide (IV), ($C_{12}H_{28}O_4Ti$)) was mixed with 40 mL of a mixture of acetic acid and ethanol (v/v = 25:75), and this mixture was aged for 1 h. Then, a corresponding amount of iron precursor was dissolved in 10 mL of distilled water and aged for a few minutes. Next, this lalter mixture was added dropwise to the first solution containing the titania precursor. The obtained solution was aged for 72 h at ambient temperature. The obtained sol was dried at 373 K for 7 days and finally calcined in air at 673 K (10 K/min).

Characterization techniques

The chemical composition of the samples was determined by inductively coupled plasma optical emission spectroscopy (ICP ES) using a Varian ICP OES instrument. The average crystallite sizes of all the samples were estimated by the Debye–Scherrer equation $d = \lambda/(\beta\cos\theta)$, where d is the TiO_2–Fe_2O_3 crystallite size, λ is the wavelength of X-rays (1.5406 Å), β is the corrected full width at half-maximum, and θ is the Bragg diffraction angle.[43] The specific surface area was determined from N_2 adsorption/desorption isotherms at 77 K using a Quantachrom NOVA 1000 instrument. Prior to the adsorption measurements, the sample was outgassed at 523 K for 2.5 h.

The UV–vis spectra (200–800 nm) of these samples were recorded on a Perkin Elmer spectrometer with an integrating sphere. The baseline was recorded using MgO as reference. The FTIR spectra of the solid samples were recorded using an Agilent Technology Cary 60 series FTIR spectrometer, with ATR accessories, and a measuring range of 4000–400 cm^{-1}.

Catalytic tests

The catalytic test of cyclohexene oxidation by molecular oxygen was carried out in a Parr 5500 series compact reactor (capacity = 0.14 L, maximum pressure 200 bar) as a function of the temperature (Parr controller) and stirring. In a typical oxidation reaction, 4.5 mL cyclohexene, 75 mL *n*-heptane, and 0.1 g of the catalyst were placed in the reactor. The reactor was closed and purged three times for air elimination. It was then heated up to 353 K. When the desired temperature was reached, molecular oxygen was introduced (P = 6 bar) under stirring. The reaction was maintained under stirring for 24 h. The reaction products were analyzed by gas chromatography (GC).

Cyclohexene conversion, selectivity, and turnover frequency were calculated using the following equations:

$$\text{Conversion}\,(\%) = \frac{n_{\text{initial}} - n_{\text{final}}}{n_{\text{initial}}}.100$$

$$\text{Selectivity}\,(\%) = \frac{\text{moles of individual product}}{\text{moles of total products}}.100$$

Turnover frequency (TOF) of methanol was calculated by the following formula:

$$\text{TOF} = \frac{n_{\text{initial}} - n_{\text{final}}}{\text{Time(s)}.\text{Weight of catalyst (g)}}$$

where n_{initial} and n_{final} are the number of moles of cyclohexene at the beginning and end of the reaction, respectively, and n_{product} is the number of moles of the product.

REFERENCES

1. J. M. Fraile, J. I. García, J. A. Mayoral, L. Salvatella, E. Vispe, D. R. Brown, G. Fuller, *J. Phys. Chem. B.* **2003**, *107*, 519.
2. C.-H. Tung, L.-Z. Wu, Z.-Y. Yuan, J.-Q. Guan, Y. Yun-Ming, H.-W. Wang, X.-H. Xu, *Mater. Sci. Eng. C* **1999**, *10*, 75.
3. R. R. Khojasteh, K. Yavangi, *J. Mater. Sci. Eng. A* **2012**, *2*, 210.
4. E. M. Serwicka, J. Połtowicz, K. Bahranowski, Z. Olejniczak, W. Jones, *Appl. Catal. A. Gen.* **2004**, *275*, 9.
5. Z.-Y. Cai, M.-Q. Zhu, J. Chen, Y.-Y. Shen, J. Zhao, Y. Tang, X.-Z. Chen, *Catal. Commun.* **2010**, *12*, 197.

 © 2017 The Chemical Society Located in Taipei & Wiley-VCH Verlag GmbH & Co. KGaA, Weinheim

6. X. Cai, H. Wang, Q. Zhang, J. Tong, Z. Lei, *J. Mol. Catal. A Chem.* **2014**, *383*, 217.
7. L. Barrio, P. Toribio, J. Campos-Martin, J. Fierro, *Tetrahedron* **2004**, *60*, 11527.
8. N. Patil, R. Jha, B. Uphade, S. Bhargava, V. Choudhary, *Appl. Catal. A Gen.* **2004**, *275*, 87.
9. H.-Y. Wu, X.-L. Zhang, C.-Y. Yang, X. Chen, X.-C. Zheng, *Appl. Surf. Sci.* **2013**, *270*, 590.
10. R. Radman, A. Aouissi, A. Al Kahtani, W. Mekhamer, *Petrol. Chem.* **2017**, *57*, 79.
11. P. Bujak, P. Bartczak, J. Polanski, *J. Catal.* **2012**, *295*, 15.
12. K. Sato, M. Aoki, R. Noyori, *Science* **1998**, *281*, 1646.
13. M. Damm, B. Gutmann, C. O. Kappe, *ChemSusChem* **2013**, *6*, 978.
14. M. Shang, T. Noël, Q. Wang, V. Hessel, *Chem. Eng. Technol.* **2013**, *36*, 1001.
15. M. D. Hughes, X. Yi-Jun, P. Jenkins, P. McMorn, *Nature* **2005**, *437*, 1132.
16. D. Gournis, M. Louloudi, M. Karakassides, C. Kolokytha, K. Mitopoulou, N. Hadjiliadis, *Mater. Sci. Eng. C* **2002**, *22*, 113.
17. S. O. Lee, R. Raja, K. D. Harris, J. M. Thomas, B. F. Johnson, G. Sankar, *Angew. Chem.* **2003**, *115*, 1558.
18. C. A. Henriques, A. Fernandes, L. M. Rossi, M. F. Ribeiro, M. J. F. Calvete, M. M. Pereira, *Adv. Funct. Mater.* **2016**, *26*, 3359.
19. A. Castellan, J. C. J. Bart, S. Cavallaro, *Catal. Today* **1991**, *9*, 237.
20. T. Mazari, S. Benadji, A. Tahar, L. Dermeche, C. Rabia, *J. Mater. Sci. Eng. B* **2013**, *3*, 146.
21. K. C. Hwang, A. Sagadevan, *Science* **2014**, *346*, 1495.
22. G. Colón, M. Maicu, M. Hidalgo, J. Navío, A. Kubacka, M. Fernández-García, *J. Mol. Catal. A Chem.* **2010**, *320*, 14.
23. M. A. Kebede, N. K. Scharko, L. E. Appelt, J. D. Raff, *J. Phys. Chem. Lett.* **2013**, *4*, 2618.
24. A. P. Surzhikov, E. N. Lysenko, V. A. Vlasov, A. V. Malyshev, M. Korobeynikov, M. Mikhailenko, *IOP Conf. Ser. Mater. Sci. Eng.* **2017**, *168*, 012090.
25. M. I. Qadir, J. D. Scholten, J. Dupont, *J. Mol. Catal. A Chem.* **2014**, *383*, 225.
26. B. Han, N. Chen, D. Deng, S. Deng, I. Djerdj, Y. Wang, *Anal. Methods* **2015**, *7*, 10052.
27. M. Ahmed, E. E. El-Katori, Z. H. Gharni, *J. Alloys Compd.* **2013**, *553*, 19.
28. L. Fan, J. Dongmei, M. Xueming, *J. Alloys Compd.* **2009**, *470*, 375.
29. M. Zhou, J. Yu, B. Cheng, *J. Hazard. Mater.* **2006**, *137*, 1838.
30. X. Gao, I. E. Wachs, *Catal. Today* **1999**, *51*, 233.
31. M. Cozzolino, M. Di Serio, R. Tesser, E. Santacesaria, *Appl. Catal. Gen.* **2007**, *325*, 256.
32. E. A. Cloutis, K. A. McCormack, J. F. Bell, A. R. Hendrix, D. T. Bailey, M. A. Craig, S. A. Mertzman, M. S. Robinson, M. A. Riner, *Icarus* **2008**, *197*, 321.
33. A. De Stefanis, S. Kaciulis, L. Pandolfi, *Microporous Mesoporous Mater.* **2007**, *99*, 140.
34. Y. Lu, J. Zheng, J. Liu, J. Mu, *Microporous Mesoporous Mater.* **2007**, *106*, 28.
35. Y. Wang, Q. Zhang, T. Shishido, K. Takehira, *J. Catal.* **2002**, *209*, 186.
36. D. Prieto-Centurion, A. M. Boston, J. M. Notestein, *J. Catal.* **2012**, *296*, 77.
37. W. Choi, A. Termin, M. R. Hoffmann, *Angew. Chem. Int. Ed. Eng.* **1994**, *33*, 1091.
38. J. Yang, J. Zhang, L. Zhu, S. Chen, Y. Zhang, Y. Tang, Y. Zhu, Y. Li, *J. Hazard. Mater.* **2006**, *137*, 952.
39. S. C. Pillai, P. Periyat, R. George, D. E. McCormack, M. K. Seery, H. Hayden, J. Colreavy, D. Corr, S. J. Hinder, *J. Phys. Chem. C* **2007**, *111*, 1605.
40. Y. Chang, Y. Lv, F. Lu, F. Zha, Z. Lei, *J. Mol. Catal. A Chem.* **2010**, *320*, 56.
41. R. Noyori, M. Aoki, K. Sato, *Chem. Commun.* **2003**, *16*, 1977.
42. T. Kundu, M. Mukherjee, D. Chakravorty, T. Sinha, *J. Mater. Sci.* **1998**, *33*, 1759.
43. A. S. Reddy, C.-Y. Chen, C.-C. Chen, S.-H. Chien, C.-J. Lin, K.-H. Lin, C.-L. Chen, S.-C. Chang, *J. Mol. Catal. A Chem.* **2010**, *318*, 60.

 © 2017 The Chemical Society Located in Taipei & Wiley-VCH Verlag GmbH & Co. KGaA, Weinheim